Progress In Electromagnetics Research, Vol. 172, 33–40, 2021

Non-Hermitian Skin Effect and Delocalized Edge States in Photonic Crystals with Anomalous Parity-Time Symmetry

Qinghui Yan[1, 2], Hongsheng Chen[1, 2, *], and Yihao Yang[1, 2, *]

Abstract—Non-Hermitian skin effect denotes the exponential localization of a large number of eigen-states at boundaries in a non-Hermitian lattice under open boundary conditions. Such a non-Hermiticity-induced skin effect can offset the penetration depth of in-gap edge states, leading to counterintuitive delocalized edge modes, which have not been studied in a realistic photonic system such as photonic crystals. Here, we analytically reveal the non-Hermitian skin effect and the delocalized edge states in Maxwell's equations for non-Hermitian chiral photonic crystals with anomalous parity-time symmetry. Remarkably, we rigorously prove that the penetration depth of the edge states is inversely proportional to the frequency and the real part of the chirality. Our findings pave a way towards exploring novel non-Hermitian phenomena and applications in continuous Maxwell's equations.

1. INTRODUCTION

Non-Hermitian skin effect (NHSE), the exponential localization of an extensive number of eigen-states at the open boundaries of the system, has gained rapidly growing attention in non-Hermitian physics. Initially proposed in condensed-matter systems under tight-binding approximation, NHSE has been theoretically constructed and experimentally realized across multiple disciplines [1–11]. So far, most studies have been focused on the NHSE in one-dimensional (1D) systems, where the conventional bulk-edge correspondence principle is violated. To recover the bulk-edge correspondence, the generalized Brillouin zone (GBZ) has been proposed, in which a nonzero imaginary part is assigned to the Bloch wavevector k [12]. The relation between $\mathrm{Re}(k)$ and $\mathrm{Im}(k)$ is thus the GBZ, with $\mathrm{Re}(\cdot)$ and $\mathrm{Im}(\cdot)$ denoting the real and imaginary parts of the inputs, respectively. Moreover, GBZ provides an intuitive picture to understand the penetration depths of the localized states.

NHSE has challenged our conventional understanding of bulk/edge states, as bulk states can be localized at the edge, whereas the edge states can be fully delocalized into states that are extended in the bulk [13]. However, they can still be distinguished by the number of eigen-states; for a lattice sized N, the number of bulk states is $O(N)$, while the number of edge states is $O(1)$ [14, 15]. In the context of photonics, the delocalized edge states (DESs) have potentials in applications. For example, due to the frequency isolation and energy delocalization, DESs manifest themselves as ideal resonant modes for single-mode lasing. While most previous studies on NHSE and DESs have been restricted to tight-binding models, realistic photonic systems such as photonic crystals usually cannot be modeled discretely. It thus requires a continuum approach based on the Maxwell's equations, which have not been studied yet.

Received 16 November 2021, Accepted 22 December 2021, Scheduled 24 December 2021

* Corresponding author: Hongsheng Chen (hansomchen@zju.edu.cn), Yihao Yang (yangyihao@zju.edu.cn).

[1] Interdisciplinary Center for Quantum Information, State Key Laboratory of Modern Optical Instrumentation, ZJU-Hangzhou Global Scientific and Technological Innovation Center, Zhejiang University, Hangzhou 310027, China. [2] International Joint Innovation Center, Key Lab. of Advanced Micro/Nano Electronic Devices & Smart Systems of Zhejiang, The Electromagnetics Academy at Zhejiang University, Zhejiang University, Haining 314400, China.

Here, we analytically study the NHSE and DESs in 1D non-Hermitian chiral PhCs based on the first-principle calculation by Maxwell's equations. We start with a Hermitian PhC and derive the eigen-spectra under periodic boundary condition (PBC) and open boundary condition (OBC), respectively. By adopting the transfer matrix method (TMM), we find that by varying the non-Hermitian chirality of one type of layers, we precisely control the penetration depth of NHSE, resulting in DESs. Finally, we prove the non-Hermitian chiral material satisfies anomalous parity-time symmetry and discuss how the real and imaginary parts of the chirality affect the dispersion relations and mode profiles, respectively.

2. HERMITIAN PHOTONIC CRYSTALS

We start with a piece of Hermitian 1D PhCs with a unit-cell consisting of two layers, namely layer A and layer B. The thicknesses of the two layers are $d_A = 2d_B = \frac{2}{3}d$, where d is the lattice constant normalized to 1. The constitutive parameters are $\epsilon_B = 4$ and $\epsilon_A = \mu_A = \mu_B = 1$, respectively. For simplicity, we suppose $\epsilon_0 = \mu_0 = c = 1$ and only consider the TE polarization with a magnetic field out of plane, as shown in Fig. 1(c). Analytically, we obtain the dispersion relation of the PhCs [16],

$$\cos[kd] = \frac{\eta+1}{2}\cos[\omega(n_A d_A + n_B d_B)] + \frac{-\eta+1}{2}\cos[\omega(n_A d_A - n_B d_B)] \tag{1}$$

The band structure of the PhC under PBC is shown in Fig. 1(a). Here, $\eta = (Z_A/Z_B + Z_B/Z_A)/2$, and $Z_{A,B}$ and $n_{A,B}$ are the impedances and refractive indices of layer A and B, respectively. For isotropic materials, $Z = \sqrt{\mu/\epsilon}$ and $n = \sqrt{\epsilon\mu}$, so $n_B = 2$, $Z_B = 1/2$ and $n_A = Z_A = 1$, and thus $\eta = 5/4$. Note that $n_A d_A - n_B d_B = 0$, which simplifies Eq. (1) to make all bands periodically arranged in the frequency domain, with a normalized periodicity $\omega_0/(c/d) = 3\pi/2$. Each period contains two bands and a bandgap in between, as shown in Fig. 1(a).

Next, we study the OBC eigen-spectra. Consider a Fabry-Pérot (FP) cavity filled with such PhCs. The cavity is bounded by perfect metals that shield the electric field, analogous to the OBC in lattice models. As shown in Fig. 1(b), the OBC spectra are almost the same as PBC counterparts, except several frequency isolated states in the middle of the bandgap, known as in-gap edge states. In our example, the finite-size PhC starts with layer A and ends with layer B, so there is only one edge state localized at the right boundary. Because of the OBC, every eigen-state is a standing wave that interferes destructively at the boundaries, mostly by two bulk states under PBC with opposite wavevectors, shown as the solid red dots and in-band red line in Fig. 1(a), and the mode profile in Fig. 1(d). Besides most bulk states, an OBC state can be destructively interfered by itself, such as the edge state located in the

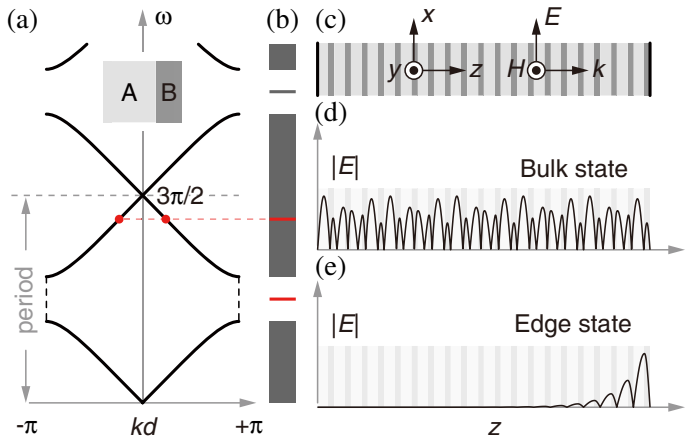

Figure 1. Hermitian PhCs. (a) Dispersion relation of PhCs under PBC. By judiciously designing the unit-cell, all bands are periodically arranged in the frequency domain, containing one bandgap in each period. The inset shows the unit-cell. (b) OBC spectra in an FP cavity. In the middle of each bandgap, there is an edge state localized at the right boundary. (c) Schematic of the PhCs under OBC. (d) Mode profile of a bulk state, shown as in-band red line in (a). (e) Mode profile of the in-gap edge state localized at the right boundary.

bandgap, having no correspondence to the PBC states. Substituting $\omega = \omega_0/2$ into Eq. (1), we have $k = \pi + ig_0$, where $g_0 = -a\cosh\eta$. Here, $g_0 < 0$ implies the rightward localization of edge state. The penetration depth is $\delta_0 = 1/|g_0| \approx 1.44$ periods.

3. GENERALIZED BRILLOUIN ZONE CALCULATED FROM TRANSFER MATRIX METHOD

For future analysis, we briefly recall TMM to describe our model. The electromagnetic field in each layer consists of two planewaves propagating forward and backward, described by the TE component of the Maxwell's equations

$$k\begin{bmatrix}0 & 1\\ 1 & 0\end{bmatrix}\begin{bmatrix}E_x\\ H_y\end{bmatrix} = \omega\begin{bmatrix}\epsilon_{xx} & \xi_{xy}\\ \zeta_{yx} & \mu_{yy}\end{bmatrix}\begin{bmatrix}E_x\\ H_y\end{bmatrix}. \tag{2}$$

Rewrite it as $n\sigma_1\Psi = \mathcal{M}\Psi$ for brief notations, where $n = k/\omega$ is the definition of refractive index, and σ_1 is the first Pauli matrix. By solving this generalized eigen-value problem, we have two eigen-values $n_\pm$ and two eigen-vectors $\Psi_\pm$, respectively, where the plus-minus sign denotes the forward/backward propagation direction. Arranging Ψ_+ and Ψ_- in columns, we have

$$\tilde{\Psi} = [\Psi_+ \quad \Psi_-] = \begin{bmatrix}Z_+ & Z_-\\ 1 & -1\end{bmatrix}. \tag{3}$$

In this work, we suppose $Z_+ = Z_-$ and suppress the plus/minus subscript of impedances. From the definition of $\tilde{\Psi}$ we have $\sigma_1\tilde{\Psi}\tilde{n} = \mathcal{M}\tilde{\Psi}$, where $\tilde{n} = \left[\begin{smallmatrix}n_+ & \\ & -n_-\end{smallmatrix}\right]$), which finally leads to

$$\mathcal{M} = \sigma_1\tilde{\Psi}\tilde{n}\tilde{\Psi}^{-1}. \tag{4}$$

In doing so, we can calculate the refractive index and impedance from the constitutive parameters, and vice versa. Take layer A as an example, and the electromagnetic field in inside the layer is expressed by

$$\begin{bmatrix}E_x\\ H_y\end{bmatrix} = \begin{bmatrix}Z_A & Z_A\\ 1 & -1\end{bmatrix}\begin{bmatrix}m_+\\ m_-\end{bmatrix} \Rightarrow \Psi = \tilde{\Psi}_A\Phi, \tag{5}$$

where m_+ and m_- are the coefficients of planewaves. Given the thickness d_A of the layer, we have

$$\Phi_{d_A} = \begin{bmatrix}e^{+i\omega n_{A+}d_A} & \\ & e^{-i\omega n_{A-}d_A}\end{bmatrix}\Phi_0 \Rightarrow \Phi_{d_A} = \mathbf{T}_A\Phi_0, \tag{6}$$

where the subscript denotes the position of the wavefunction. $n_{A\pm}$ denotes the refractive index for the forward/backward component, which is not the same in chiral materials. Given that the electromagnetic field is continuous along the interface between every two neighboring layers, we have

$$(\tilde{\Psi}_B\mathbf{T}_B\tilde{\Psi}_B^{-1})(\tilde{\Psi}_A\mathbf{T}_A\tilde{\Psi}_A^{-1})\Psi_0 = \Psi_d = \beta\Psi_0 \tag{7}$$

for the unit-cell under Floquet boundary condition, where $\beta = e^{ikd}$ is the generalized phase shift per unit-cell. Here, the *generalized* means k can have nonzero imaginary part to amplify/attenuate the amplitude of the wave. By solving this eigen-value problem, we find two eigen-values, namely β_+ and β_-, both leading to Eq. (1), the characteristic equation of the PhCs.

Then, we consider the formulae of PBC and OBC, which lead to similar spectra in Hermitian systems but have different physical meanings in essence. The former supposes that all the unit-cells are connected from head to tail to preserve the energy flux along the propagation direction, enforcing k to be a real number and thus $|\beta| = 1$; the latter supposes that the PhCs are bounded by two mirrors at which the wavefunctions are destructively interfered, which in most cases involves two Bloch states to form a standing wave. Note that the wavevectors of the two states are not required to be real numbers. As N is sufficiently large, both spectra become continuous point sets that form closed 1D loops over the complex plane of frequency, respectively. The loop of OBC spectra covers zero area, surrounded by the PBC spectra covering nonzero area with a nontrivial winding number [15]. To derive the relation between the two wavevectors, we write down the electric field in the FP cavity

$$E_x = Z_A m_+\beta_+^N + Z_A m_-\beta_-^N, \tag{8}$$

and apply perfect metal boundaries to both sides ($z = 0$ and Nd). As a result, we have

$$\beta_+^N = \beta_-^N, \text{ or } k_+ - k_- = \frac{2\pi M}{Nd}, \tag{9}$$

where M is an integer denoting the number of half waves in the cavity. As N is sufficiently large (thermodynamic limit), $2\pi M/(Nd)$ can be an arbitrary real number so that

$$|\beta_+| = |\beta_-|, \text{ or } \mathrm{Im}(k_+) = \mathrm{Im}(k_-), \tag{10}$$

meaning that the exponential decays of the forward and backward waves are the same, so as to satisfy the OBCs at arbitrary length of the cavity. By solving Eq. (10), we have the GBZ of the PhCs. For previous example with Hermiticity, k is always a real number for the bulk states, and therefore, GBZ overlaps with the Brillouin zone (BZ). Note that Eq. (10) does not work for the edge states that are self destructively interfered.

4. NON-HERMITIAN SKIN EFFECT AND DELOCALIZED EDGE STATES IN ANOMALOUS PARITY-TIME SYMMETRIC PHOTONIC MATERIAL

Based on the TMM, the NHSE can be achieved in a tricky way. Without loss of generality, we multiply both sides of Eq. (7) by a nonzero complex coefficient e^{-gd}, which is

$$\tilde{\Psi}_B(e^{-gd}\mathbf{T}_B)\tilde{\Psi}_B^{-1}\tilde{\Psi}_A\mathbf{T}_A\tilde{\Psi}_A^{-1}\Psi = (e^{-gd}\beta)\Psi, \tag{11}$$

and suppose $\mathbf{T}_{B'} = e^{-gd}\mathbf{T}_B$ and $\beta' = e^{-gd}\beta$ to have a new layer B' and generalized phase shift β' to satisfy Eqs. (10) and (11) under OBC. Correspondingly, $n_{B'\pm} = n_B \pm ig/(\omega d_B)$ and $k' = k + ig$. The transform does not affect ω and Ψ, so the OBC spectra and Zak phase [17] are preserved; the only change is the dispersion relation between ω and k'. Especially, we note that as $\mathrm{Re}(g) \neq 0$, $|\beta'| \neq 1$, all the Bloch states become evanescent, resulting in the NHSE. The decay rate is $\mathrm{Im}(k') = \mathrm{Re}(g)$ for the bulk states, and $\mathrm{Im}(k') = \mathrm{Re}(g) + g_0$ for the edge states. Substituting the new refractive indices into Eq. (4), we have

$$\mathcal{M} = \begin{bmatrix} \dfrac{n_+ + n_-}{2Z} & \dfrac{n_+ - n_-}{2} \\ \dfrac{n_+ - n_-}{2} & \dfrac{(n_+ + n_-)Z}{2} \end{bmatrix} = \begin{bmatrix} \epsilon & i\kappa \\ i\kappa & \mu \end{bmatrix}, \tag{12}$$

where the chirality term $\kappa = g/(\omega d_B)$. Correspondingly, the penetration depths of bulk states and edge states are

$$\delta_{\text{bulk}} = \frac{1}{|d_B \mathrm{Re}(\kappa)\omega|} \tag{13}$$

and

$$\delta_{\text{edge}} = \frac{1}{|d_B \mathrm{Re}(\kappa)\omega - 1/\delta_0|}, \tag{14}$$

respectively. One can see that the penetration depth is tuned by κ and ω. For $\mathrm{Re}(\kappa) > 0$, all states tend to be localized leftwards. As the frequency increases, the localizations of bulk states become stronger in a linear pattern, leading to smaller penetration depths that are inversely proportional to frequency. For the edge states, it takes a range of frequency from $\omega = 0$ to $1/(\delta_0 d_B \mathrm{Re}(\kappa))$ to offset the intrinsic rightward localizations, where the penetration depth increases from δ_0 to infinity. By choosing proper values of κ, the penetration depth happens to be infinite for some edge states, giving rise to the DES. As shown in Fig. 2, we plot the mode profiles of each eigen-state for $\kappa = 0$ and $\kappa = 1/(2.5\omega_0\delta_0 d_B)$, and the latter has DES at the third bandgap. For each state we mark the penetration depth by solid points where the wavefunction is $1/e$ decayed from the boundary. As shown in Fig. 2(b), all the points are set on the hyperbolic curves satisfying either Eqs. (13) or (14). The third edge state is exactly at the asymptotic line of two branches, doubly confirming the delocalization. As a comparison in Fig. 2(a), the system is Hermitian; the bulk states are extensive in the real space; and every edge state has δ_0 skin depth to the right end.

From Eq. (12) we see that the material matrix is transpose symmetric, meaning that the material of layer B' satisfies the anomalous parity-time ($\mathcal{HPT}$) [18] symmetry. Here, $\mathcal{H}$, $\mathcal{P}$, and $\mathcal{T}$ denote

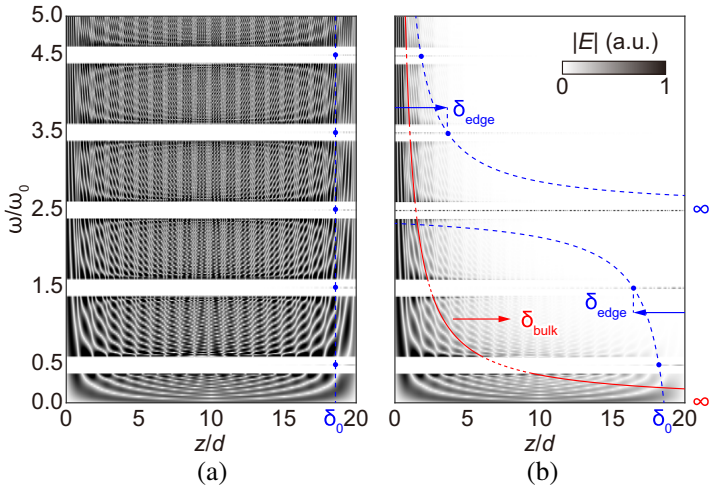

Figure 2. Mode profiles of eigen-states in a piece of non-Hermitian PhCs with 20 unit-cells. (a) $\kappa = 0$. All bulk states are extensive in the cavity, while all edge states are intrinsically localized at the right end with penetration depth δ_0. (b) $\kappa = 1/(2.5\omega_0\delta_0 d_B)$. All bulk states are localized leftwards. The edge states are localized rightwards as $0 < \omega < 2.5\omega_0$ and leftwards as $\omega > 2.5\omega_0$. At $\omega = 2.5\omega_0$, the third edge state is delocalized. The penetration depths of all states are on three branches of hyperbolic curves, described by Eqs. (13) and (14), respectively.

Table 1. Representations of Hermiticity, TRS, inversion symmetry, and some combinations of them. Note $\mathcal{R}$ is the reciprocity operator. Constraints on the material matrix and constitutive parameters are also listed.

Symmetry	Wavefunction	Material matrix	Constitutive parameters
$\mathcal{H}$	$\begin{bmatrix} E_x \\ H_y \end{bmatrix} \to \begin{bmatrix} E_x^*, H_y^* \end{bmatrix}$	$\mathcal{M} = \mathcal{M}^\dagger$	$\epsilon = \epsilon^*$, $\mu = \mu^*$ $\xi = \zeta^*$
$\mathcal{T}$	$\begin{bmatrix} E_x \\ H_y \end{bmatrix} \to \begin{bmatrix} E_x^* \\ -H_y^* \end{bmatrix}$	$\mathcal{M} = \sigma_3 \mathcal{M}^* \sigma_3$	$\epsilon = \epsilon^*$, $\mu = \mu^*$ $\xi = -\xi^*$, $\zeta = -\zeta^*$
$\mathcal{P}$	$\begin{bmatrix} E_x \\ H_y \end{bmatrix} \to \begin{bmatrix} -E_x \\ H_y \end{bmatrix}$	$\mathcal{M} = \sigma_3 \mathcal{M} \sigma_3$	$\xi = \zeta = 0$
$\mathcal{R} = \mathcal{HT}$	$\begin{bmatrix} E_x \\ H_y \end{bmatrix} \to \begin{bmatrix} E_x, -H_y \end{bmatrix}$	$\mathcal{M} = \sigma_3 \mathcal{M}^T \sigma_3$	$\xi = -\zeta$
$\mathcal{PT}$	$\begin{bmatrix} E_x \\ H_y \end{bmatrix} \to \begin{bmatrix} -E_x^* \\ -H_y^* \end{bmatrix}$	$\mathcal{M} = \mathcal{M}^*$	$\epsilon = \epsilon^*$, $\mu = \mu^*$ $\xi = \xi^*$, $\zeta = \zeta^*$
$\mathcal{HP}$	$\begin{bmatrix} E_x \\ H_y \end{bmatrix} \to \begin{bmatrix} -E_x^*, H_y^* \end{bmatrix}$	$\mathcal{M} = \sigma_3 \mathcal{M}^\dagger \sigma_3$	$\epsilon = \epsilon^*$, $\mu = \mu^*$ $\xi = -\zeta^*$
$\mathcal{HPT}$	$\begin{bmatrix} E_x \\ H_y \end{bmatrix} \to \begin{bmatrix} -E_x^*, -H_y^* \end{bmatrix}$	$\mathcal{M} = \mathcal{M}^T$	$\xi = \zeta$

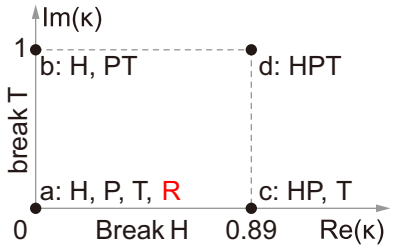

Figure 3. Complex plane of κ, where we pick four points (corresponding to Figs. 4(a)–(d)) and label the symmetries in each case, respectively.

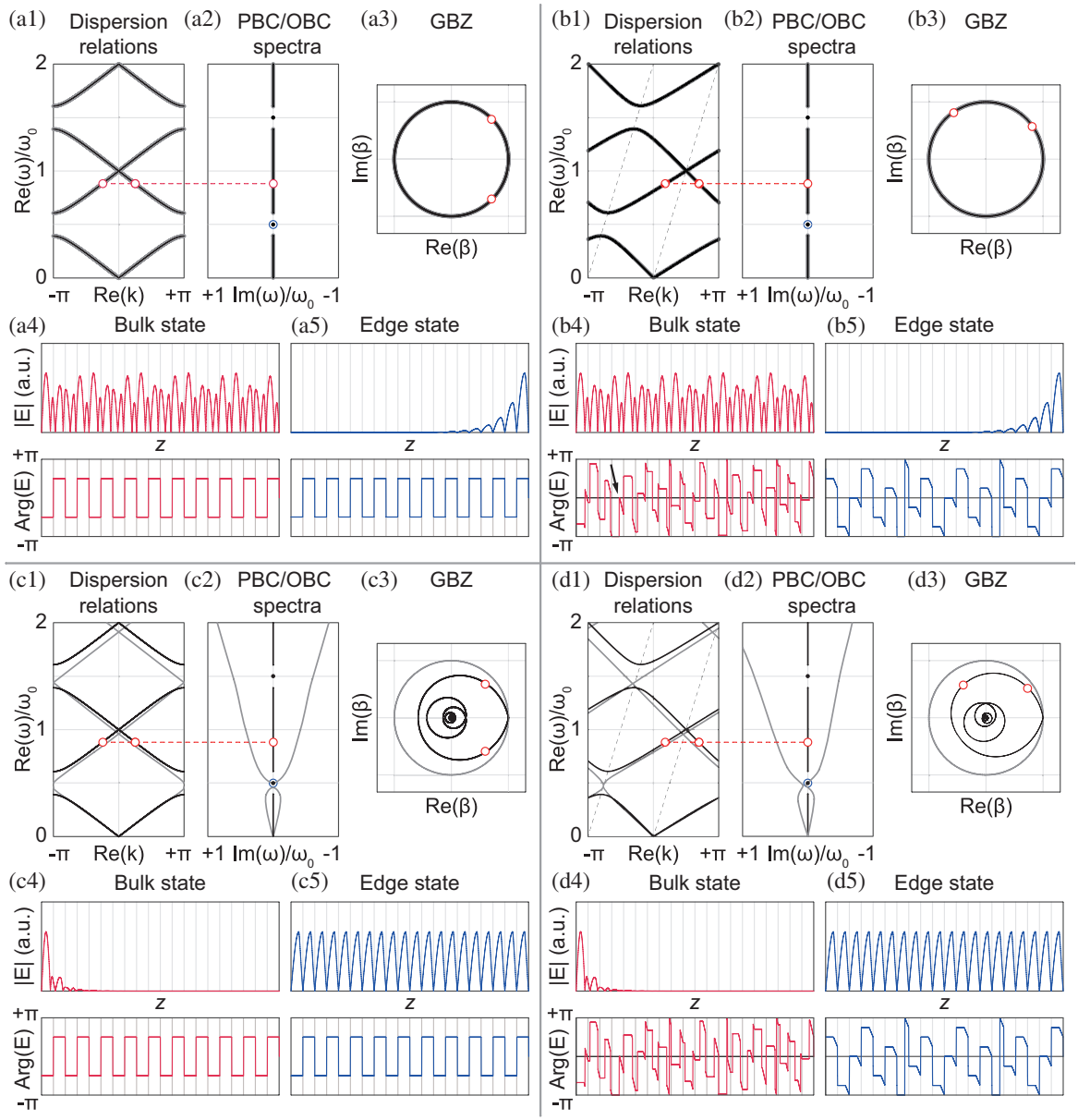

Figure 4. Band diagrams of four cases of κ in Fig. 3. (a) $\kappa = 0$, same as Fig. 1. (a1), (a2) Due to the Hermiticity, the PBC/OBC spectra are rigorous real numbers and almost the same, except discrete edge states in the bandgaps. Empty circles in (a2) denotes the standing wave under OBC that consists of two states under PBC. (a3) Complete overlap of BZ and GBZ. (a4) Mode profile of a bulk state. (a5) Mode profile of the first edge state localized at the right end. (b) $\kappa = i$. The system remains Hermitian (b1) with an offset of wavevectors proportional to frequency, denoted by the dashed line. (b4), (b5) Mode profiles of bulk and edge states. The phase shift is progressive along the unit-cells. (c) $\kappa = -0.89$. Due to the preservation of TRS, the PBC/OBC spectra and GBZs are complex conjugate to themselves, respectively. (c1), (c2) Because of the non-Hermiticity, PBC and OBC spectra no long overlap. The first edge state locates at the contour of PBC spectra, indicating the delocalization. (c3) All the GBZs lie inside the BZ, implying (c4) the leftward localization. (c5) DES. (d) $\kappa = -0.89 + i$. (d1), (d2) Despite the breaking of TRS, the first edge state is still at the contour of PBC spectra. (d3) GBZs of each band is no longer complex conjugate to themselves, but rotates around the original point of β. (d4), (d5) Mode profiles of NHSE and DES with progressive phases.

the Hermiticity, inversion symmetry, and time-reversal symmetry (TRS) operators, respectively; the anomalous parity-time symmetry is the multiplication of the three symmetry operators.

To prove that material B' satisfies $\mathcal{HPT}$ symmetry, we refer to the symmetry analysis. Given a system described by the Maxwell's equations $\mathcal{D}\Psi = \omega\mathcal{M}\Psi$ and a symmetry operator $\mathcal{A}$, the system after transform $\mathcal{A}$ is $(\mathcal{A}\mathcal{D}\mathcal{A}^{-1})(\mathcal{A}\Psi) = (\mathcal{A}\omega\mathcal{A}^{-1})(\mathcal{A}\mathcal{M}\mathcal{A}^{-1})(\mathcal{A}\Psi)$. If the system is $\mathcal{A}$ invariant, then $\mathcal{M} = \mathcal{A}\mathcal{M}\mathcal{A}^{-1}$. As shown in Columns 2–4 in Table 1, the Hermiticity operator $\mathcal{H}$ performs the Hermitian conjugation to the wavefunction, turning a right eigen-state to a left eigen-state; the TRS operator is anti-unitary and flips the sign of the magnetic field; the inversion operator is unitary and flips the sign of the electric field. Restrictions on the material matrix invariant to the symmetries are listed in Column 3. With the three fundamental symmetries (respectively commutative), we list some combinations of them to judge the symmetry satisfaction of material B'. As shown in the complex plane of κ in Fig. 3, the material is $\mathcal{HPT}$ symmetric over the entire plane, and so long as $\kappa \neq 0$, the material is nonreciprocal. As κ is an imaginary number, the system is Hermitian and $\mathcal{PT}$ symmetric; as κ is a real number, the system satisfies TRS and anomalous inversion ($\mathcal{HP}$) symmetry.

5. TUNING PENETRATION DEPTH OF THE EDGE STATES BY CHIRALITY

To show how the NHSE and edge states are tuned by the chirality term, we choose four cases of κ (corresponding to four points in Fig. 3) to calculate the dispersion relations, the PBC/OBC spectra, the mode profiles of bulk and edge states, and the GBZs of the first four bands from zero frequency, respectively, as shown in Fig. 4. We start with $\kappa = 0$, the origin of the κ space, as shown in Fig. 4(a), which is already mentioned in Fig. 1. From Fig. 4(a) to Fig. 4(b), where κ turns into an imaginary number, the wavevector is attached with a bias $(\mathrm{Im}(\kappa)d_B/d)\omega$, performing an Arnold transform to the dispersion relation, as shown in Fig. 4(b1). Unlike the $\pm\pi/2$ phase in Figs. 4(a4), (a5), the phases in Figs. 4(b4), (b5) are progressively shifted in a linear pattern, since the Bloch states comprising the standing wave do not belong to a pair of opposite wavevectors, as shown in Fig. 4(b1). Due to the Hermiticity of PhCs, the PBC/OBC spectra is preserved, and the GBZ overlaps with BZ, which is the unit-circle in the complex plane of β.

Next, we introduce NHSE by allowing $\mathrm{Re}(\kappa) = 0.89$, which delocalize the first edge state at $\omega = \omega_0/2$. As shown in Fig. 4(c), where κ is purely a real number, both the forward and backward wavevectors are attached with an identical imaginary part to localize the states to the left boundary. Due to the non-Hermiticity, PBC and OBC spectra split apart, while the first edge state is located exactly at the contour of PBC spectra, meaning that this state does not need to add a nonzero imaginary part to the wavevector to satisfy the OBC, implying that it is a DES, as shown in Fig. 4(c5). We note that the material has $\mathcal{HP}$ symmetry [19], which is reported in another work on DES realized by tight-binding model [13]. Besides, due to the TRS, the PBC/OBC spectra and the GBZ of each band overlap with the complex conjugate of themselves, respectively.

Finally, as κ is generally a complex number, such as $\kappa = 0.89 + i$ in Fig. 4(d), both real and imaginary parts of the wavevector are tuned which result in both the progressive phase and NHSE. Despite the breaking of TRS, the eigen-frequency of every state is preserved to be real numbers, and the edge state is still on the contour of PBC spectra and therefore is delocalized.

6. DISCUSSIONS

We have thus proposed to realize the NHSE and DES in realistic photonic crystals with materials obeying anomalous Parity-time symmetry, based on the ab initio calculation on Maxwell's equations. We reveal that, in general, the penetration depth of the eigen-state is inversely proportional to the non-Hermitian chirality term κ and frequency ω, reflected as the hyperbolic curves in Fig. 2. With a careful choice of κ, the offset between the penetration depth and the intrinsic decay length of the edge state leads to the fully delocalized in-gap edge state, with eigen-frequency as a real number. This state can thus serve as an ideal resonant mode with an isolated eigen-frequency and a high-quality factor, which is useful in many aspects of photonics such as lasers, filters, and sensors. Besides, chiral material with anomalous Parity-time symmetry guarantees the non-reciprocity, which provides an alternative way to break reciprocity [20].

ACKNOWLEDGMENT

The work at Zhejiang University was sponsored by the National Natural Science Foundation of China (NNSFC) under Grants No. 61625502, No. 62175215, No. 11961141010, No. 61975176, and No. U19A2054, the Top-Notch Young Talents Program of China, and the Fundamental Research Funds for the Central Universities. The authors declare no conflicts of interest. Data underlying the results presented in this paper are not publicly available at this time but may be obtained from the authors upon reasonable request.

REFERENCES

1. Wang, K., A. Dutt, K. Y. Yang, C. C. Wojcik, J. Vučković, and S. Fan, "Generating arbitrary topological windings of a non-Hermitian band," *Science*, Vol. 371, 1240–1245, 2021.
2. Xiao, L., T. Deng, K. Wang, G. Zhu, Z. Wang, W. Yi, and P. Xue, "Non-Hermitian bulk-boundary correspondence in quantum dynamics," *Nature Physics*, Vol. 16, 761–766, 2020.
3. Helbig, T., T. Hofmann, S. Imhof, M. Abdelghany, T. Kiessling, L. Molenkamp, C. Lee, A. Szameit, M. Greiter, and R. Thomale, "Generalized bulk-boundary correspondence in non-Hermitian topolectrical circuits," *Nat. Phys.*, Vol. 16, 747–750, 2020.
4. Longhi, S., "Non-Bloch-band collapse and chiral Zener tunneling," *Phys. Rev. Lett.*, Vol. 124, 066602, 2020.
5. Zhou, D. and J. Zhang, "Non-Hermitian topological metamaterials with odd elasticity," *Phys. Rev. Research*, Vol. 2, 023173, 2020.
6. Longhi, S., "Topological phase transition in non-Hermitian quasicrystals," *Phys. Rev. Lett.*, Vol. 122, 237601, 2019.
7. Gao, P., M. Willatzen, and J. Christensen, "Anomalous topological edge states in non-Hermitian piezophononic media," *Phys. Rev. Lett.*, Vol. 125, 206402, 2020.
8. Longhi, S., "Non-bloch $\mathcal{PT}$ symmetry breaking in non-Hermitian photonic quantum walks," *Opt. Lett.*, Vol. 44, 5804–5807, 2019.
9. Deng, K. and B. Flebus, "Non-Hermitian skin effect in magnetic systems," arXiv:2109.01711, 2021.
10. Braghini, D., L. G. G. Villani, M. I. N. Rosa, and J. R. de F Arruda, "Non-Hermitian elastic waveguides with piezoelectric feedback actuation: Non-reciprocal bands and skin modes," *J. Phys. D: Appl. Phys.*, Vol. 54, 285302, 2021.
11. Song, Y., W. Liu, L. Zheng, Y. Zhang, B. Wang, and P. Lu, "Two-dimensional non-Hermitian skin effect in a synthetic photonic lattice," *Phys. Rev. Applied*, Vol. 14, 064076, 2020.
12. Yao, S. and Z. Wang, "Edge states and topological invariants of non-Hermitian systems," *Phys. Rev. Lett.*, Vol. 121, 086803, 2018.
13. Zhu, W., W. X. Teo, L. Li, and J. Gong, "Delocalization of topological edge states," *Phys. Rev. B*, Vol. 103, 195414, 2021.
14. Okuma, N., K. Kawabata, K. Shiozaki, and M. Sato, "Topological origin of non-Hermitian skin effects," *Phys. Rev. Lett.*, Vol. 124, 086801, 2020.
15. Zhang, K., Z. Yang, and C. Fang, "Correspondence between winding numbers and skin modes in non-Hermitian systems," *Phys. Rev. Lett.*, Vol. 125, 126402, 2020.
16. Xiao, M., Z. Q. Zhang, and C. T. Chan, "Surface impedance and bulk band geometric phases in one-dimensional systems," *Phys. Rev. X*, Vol. 4, 021017, 2014.
17. Zak, J., "Berry's phase for energy bands in solids," *Phys. Rev. Lett.*, Vol. 62, 2747–2750, 1989.
18. Yi, Y. and Z. Yang, "Non-Hermitian skin modes induced by on-site dissipations and chiral tunneling effect," *Phys. Rev. Lett.*, Vol. 125, 186802, 2020.
19. Okugawa, R., R. Takahashi, and K. Yokomizo, "Non-Hermitian band topology with generalized inversion symmetry," *Phys. Rev. B*, Vol. 103, 205205, 2021.
20. Buddhiraju, S., A. Song, G. T. Papadakis, and S. Fan, "Nonreciprocal metamaterial obeying time-reversal symmetry," *Phys. Rev. Lett.*, Vol. 124, 257403, 2020.